Liquid Crystals
Publication details, including instructions for authors and subscription information:
http://www.informaworld.com/smpp/title~content=t713926090

Crystallization kinetics study on higher homologues of benzylidene aniline compounds: impact of phase variant on nucleation process

P. A. Kumar; Swathi Pisupati; V. G. K. M. Pisipati; CH. Srinivasu; P. Narayana Murty

Online publication date: 11 November 2010

To cite this Article Kumar, P. A. , Pisupati, Swathi , Pisipati, V. G. K. M. , Srinivasu, CH. and Murty, P. Narayana(2002) 'Crystallization kinetics study on higher homologues of benzylidene aniline compounds: impact of phase variant on nucleation process', Liquid Crystals, 29: 7, 967 — 977
To link to this Article: DOI: 10.1080/02678290210145175
URL: http://dx.doi.org/10.1080/02678290210145175

LIQUID CRYSTALS, 2002, VOL. 29, NO. 7, 967–977

Crystallization kinetics study on higher homologues of benzylidene aniline compounds: impact of phase variant on nucleation process

P. A. KUMAR, SWATHI PISUPATI, V. G. K. M. PISIPATI*
Centre for Liquid Crystal Research and Education (CLCRE), Faculty of Physical Sciences, Nagarjuna University, Nagarjunanagar—522 510, India

CH. SRINIVASU and P. NARAYANA MURTY
Department of Physics, Nagarjuna University, Nagarjunanagar—522 510, India

(*Received 7 July 2001; in final form 9 August 2001; accepted 19 February 2002*)

A systematic kinetic study leading to the crystallization process from the kinetophases (which occur prior to crystal phase) smectic B, crystal G and smectic F is performed on representative compounds of the homologous series *p*-phenylbenzylidene-*p*′-alkylanilines (PB*n*A) and *p*-*n*-alkoxybenzylidene-*p*′-alkylanilines (*n*O.*m*) these compounds are *p*-phenylbenzylidene-*p*′-nonylaniline (PB9A), *p*-phenylbenzylidene-*p*′-tetradecylaniline (PB14A), *p*-*n*-pentadecyloxybenzylidene-*p*′-tetradecylaniline (15O.14) and *p*-*n*-octadecyloxybenzylidene-*p*′-nonylaniline (18O.9). The molecular mechanism and dimensionality in crystal growth from the kineto phases are computed from the Avrami equation, while the characteristic crystalline time (t^*) at each crystallization temperature is deduced from the individual plots of log t vs. ΔH. The low magnitudes of the dimensionality parameter n infers the occurrence of diffusion-controlled transformations leading to the formation of plates or needles of finite size possessing impinged edges. The degree of variation in the value of n at each crystallization temperature also reveals the existence of an independent nucleation mechanism for any individual member of the series. The influence of the terminal alkyl chain lengths on the rate of crystallization is determined from a comparative study with the reported analogous compounds.

1. Introduction

A wide variety of liquid crystal systems involving smectic phases have been developed during the last two decades. In recent years, considerable interest has been generated among material scientists [1–5] in the study of the kinetics of transformations in various smectogens. A large majority of polymorphic transformations, and transformations involving simple decomposition into two phase regions, are described by a process of nucleation and growth in which the nuclei of a new phase are first formed at a particular rate in the form of small domains followed by their aggregation at a faster rate resulting in the formation of layered domains. The study of crystallization kinetics has revealed to a great extent the degree of variation in layer thickness together with molecular rotation among the tilted (smectic F, crystal G) and orthogonal (smectic B) smectogens, which has a profound influence on the rate of crystallization. In continuation of our extensive crystallization kinetics investigations on the smectic layers of *N*-(*p*-*n*-alkoxybenzylidene)-*p*-*n*-alkylanilines (*n*O.*m*) compounds [6], and H-bonded mesogens [7–10], the present communication deals with a comparative crystallization kinetics study on representative compounds of the series of *p*-phenylbenzylidene-*p*′-alkylanilines (PB*n*A) and *p*-*n*-alkoxybenzylidene-*p*′-alkylanilines (*n*O.*m*) (figure 1): these are *p*-phenylbenzylidene-*p*′-nonylaniline (PB9A), *p*-phenylbenzylidene-*p*′-tetradecylaniline (PB14A), *p*-*n*-pentadecyloxybenzylidene-*p*′-tetradecylaniline (15O.14) and *p*-*n*-octadecyloxybenzylidene-*p*′-nonylaniline (18O.9).

*Author for correspondence;
e-mail: venkata_pisipati@hotmail.com

2. Experimental

2.1. *Synthesis and characterization*

The synthetic procedures for the compounds *n*O.*m* and PB*n*A are described in our earlier reports [11, 12]. The rate of growth of melting transitions and their corresponding enthalpies at each crystallization temperature were measured by a Perkin-Elmer DSC-7 system (Perkin-Elmer DSC 7). The crystallization kinetics relating

Liquid Crystals ISSN 0267-8292 print/ISSN 1366-5855 online © 2002 Taylor & Francis Ltd
http://www.tandf.co.uk/journals
DOI: 10.1080/02678290210145175

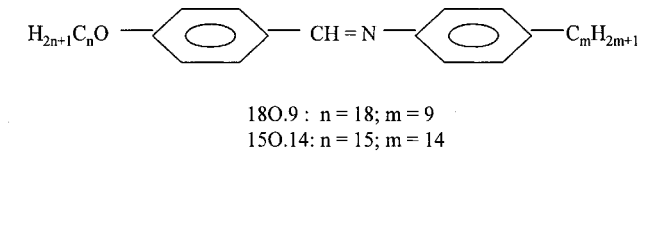

Figure 1. Molecular structures of *n*O.*m* and PB*n*A compounds.

to the phase transition from crystal to melt for each compound was selectively performed at predetermined crystallization temperatures.

A typical DSC thermal scan for a given sample at each crystallization temperature is described as follows. The sample is heated to its isotropic melt with a scanning rate of 1°C min^{-1} and, after holding for ~2 min for attaining thermal equilibrium, the sample is cooled at the same scan rate to its predetermined crystallization temperature. After holding for a given time interval at a given crystallization temperature, the endotherm peaks are recorded while the sample is heated to the isotropic state at 5°C min^{-1} scan rate. This process was repeated for each individual member of the series under present investigation, at the corresponding preselected crystallization temperature.

2.2. *Selection of thermal range of crystallization temperatures*

The procedure for the thermal selection of crystallization temperatures (CT) is described for PB9A as a representative member of the present PB*n*A series. The heating and cooling thermograms of PB9A are illustrated in figure 2. On heating, the compound exhibits four distinct transitions at 92.8°C (crystal to smectic B) (Cr–SmB), 126.1°C (smectic B to smectic A) (SmB–SmA), 131.3°C (smectic A to nematic) (SmA–N) and 133.9°C (nematic to isotropic) (N–I) with their corresponding enthalpies, 67.3, 10.0, 5.2 and 1.8 J g^{-1}, respectively. The cooling exotherm shows the corresponding transitions

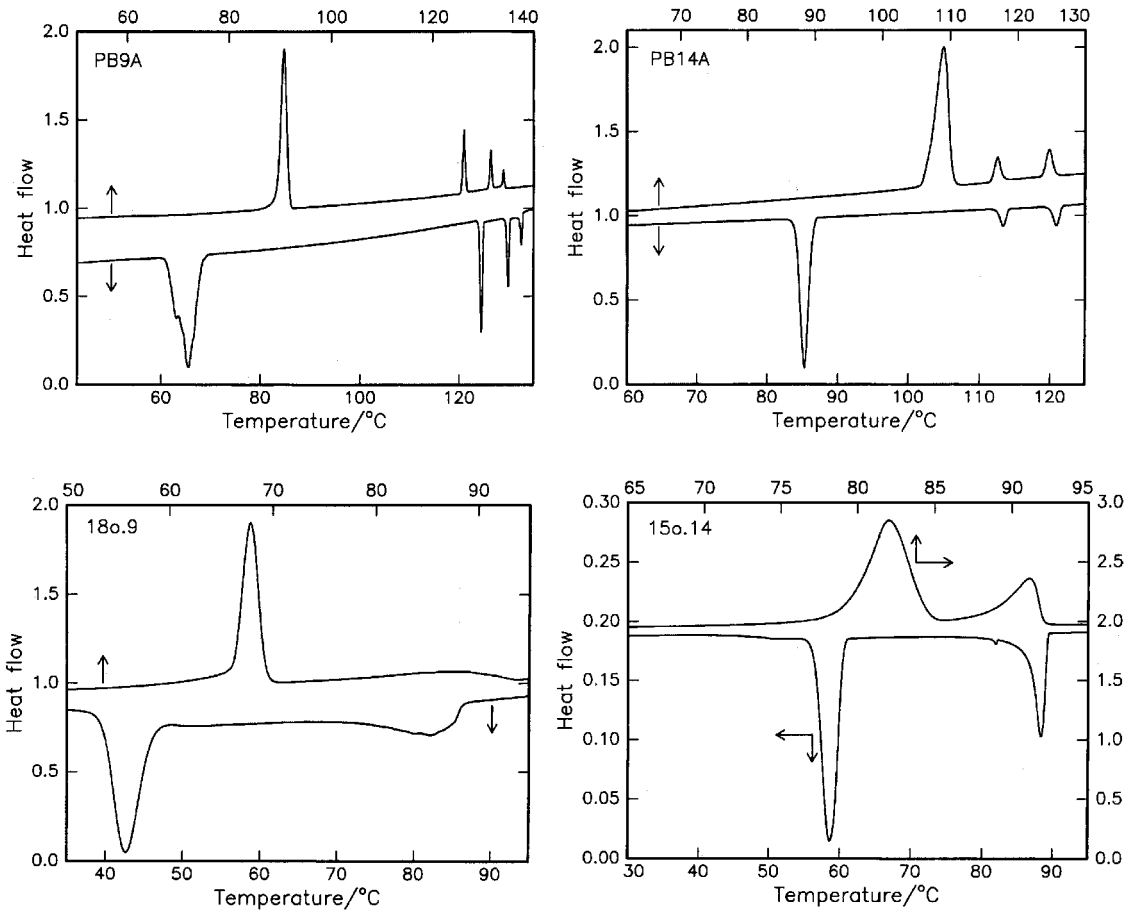

Figure 2. DSC heating and cooling thermograms of PB*n*A and *n*.O*m* compounds.

at 132.5°C (I–N), 129.8°C (N–SmA), 124.4°C (SmA–SmB) and 65.6°C (SmB–Cr) with their enthalpies 2.0, 5.1, 9.5 and 65.2 J g^{-1}, respectively. The crystallization kinetics relating to the transition from SmB was performed over the crystallization range 69–77°C. A glance at figure 2 reveals the thermal span of the mesomorphic phases as: $(T_{\text{Cr-SmB}}) - (T_{\text{SmB-Cr}}) = \sim 29$°C. Once the phase transition from SmA to SmB was complete, the kinetics of the crystallization from SmB could be investigated over the temperature range between $T_{\text{Cr-SmB}}$ and $T_{\text{SmB-Cr}}$, if the crystallization kinetics were not too fast.

DSC thermograms for the other compounds are also depicted in figure 2. The method of thermal selection of crystallization thermal ranges was adopted for the remaining compounds and the corresponding crystallization temperatures are given below.

3. Results and discussion

The phase variants in *n*O.*m* and PB*n*A were identified from their characteristic textures by cooling the isotropic melt using a polarizing thermal microscopy (TM) [13]. In these studies the *n*O.*m* compounds displayed a broken focal-conic fan texture in the SmF phase (15O.14 and 18O.9) and smooth mosaic plates in the G phase (15O.14). On the other hand, the PB*n*A members exhibited a characteristic marble texture in the N phase (PB9A), focal-conic fans in the SmA phase (PB9A and PB14A), and the appearance of transient transition bars on focal-conic fans followed by the smooth focal-conic texture in the SmB phase (PB9A and PB14A). The transition temperatures of these phases observed through TM are found to be in reasonable agreement with the data obtained from the corresponding DSC thermograms (table 1).

3.1. *Rate of crystallization*

3.1.1. *p-Phenylbenzylidene-p′-alkylanilines (PBnA)*

In order to study the impact of the alkyl chain length of the aniline moiety on the rate of crystallization, a comparative kinetics investigation was performed on two representative members of the series, *p*-phenylbenzylidene-*p′*-nonylaniline (PB9A) and *p*-phenylbenzylidene-*p′*-tetradecylaniline (PB14A).

3.1.1.1. *p-Phenylbenzylidene-p′-nonylaniline (PB9A).* Following the method of selecting the crystallization thermal ranges described in the previous section, the crystallization kinetics relating to the phase transition from SmB to crystal was selectively performed at each predetermined crystallization temperature, viz. 69, 71, 75 and 77°C. Figure 3 illustrates typical DSC endotherm profiles for different time intervals at crystallization temperatures 69 and 77°C.

The heating thermograms (figure 3) recorded after holding the compound at 69°C for different time intervals (0.1 to 2.0 min) displays three peaks corresponding to SmB–SmA, SmA–N and N–I transitions indicating the non-existence of a crystal to melting transition. The formation of a crystal to melting transition appears to begin after holding the sample for 0.8 min, suggesting a fast crystallization process. The extent of this melting transition increases with increase in time interval, and its growth continues until the time interval reaches 2.0 min. This process of crystallization can be accounted for on the basis of formation of larger and larger crystal fractions with time, complete after 2.0 min. The endotherm profiles recorded at crystallization temperatures, 71, 73 and 75°C for different time intervals reveal a similar trend of crystallization kinetics and saturated enthalpy values are obtained after 4.0, 8.0 and 8.0 min, respectively.

As expected, the thermogram recorded at $t = 0$ min at crystallization temperature 77°C exhibits all the transitions except the crystal to melting transition. The sudden appearance of the melting transition with a saturated value of enthalpy at 128.0 min suggests an altogether different trend in the formation of the melting transition. This may be

Table 1. Thermal and phase behaviour of PB*n*A and *n*O.*m* compounds. I = isotropic, N = nematic, A = smectic A, B = smectic B, F = smectic F, G = crystal G, Cr = crystalline.

		Phase transition temperatures/°C (in cooling cycle) of TM and [DSC (ΔH in J g^{-1})]				
Compound	Phase variant	I–N/A/F/G	N–A	A–B	F–G	B/F/G–Cr
PB9A	NAB	131.5 [132.5 (2.0)]	129.5 [129.8 (5.1)]	124.0 [124.4 (9.5)]		66.1 [65.6 (45.2)]
PB14A	AB	115.0 [120.9 (9.1)]		112.0 [113.3 (7.7)]		99.0 [85.3 (53.8)]
18O.9	F	82.4 [82.3 (18.9)]				43.5 [42.6 (63.4)]
15O.14	FG	88.6 [89.2 (30.3)]			86.8 [82.3 (0.2)]	59.2 [59.1 (129.5)]

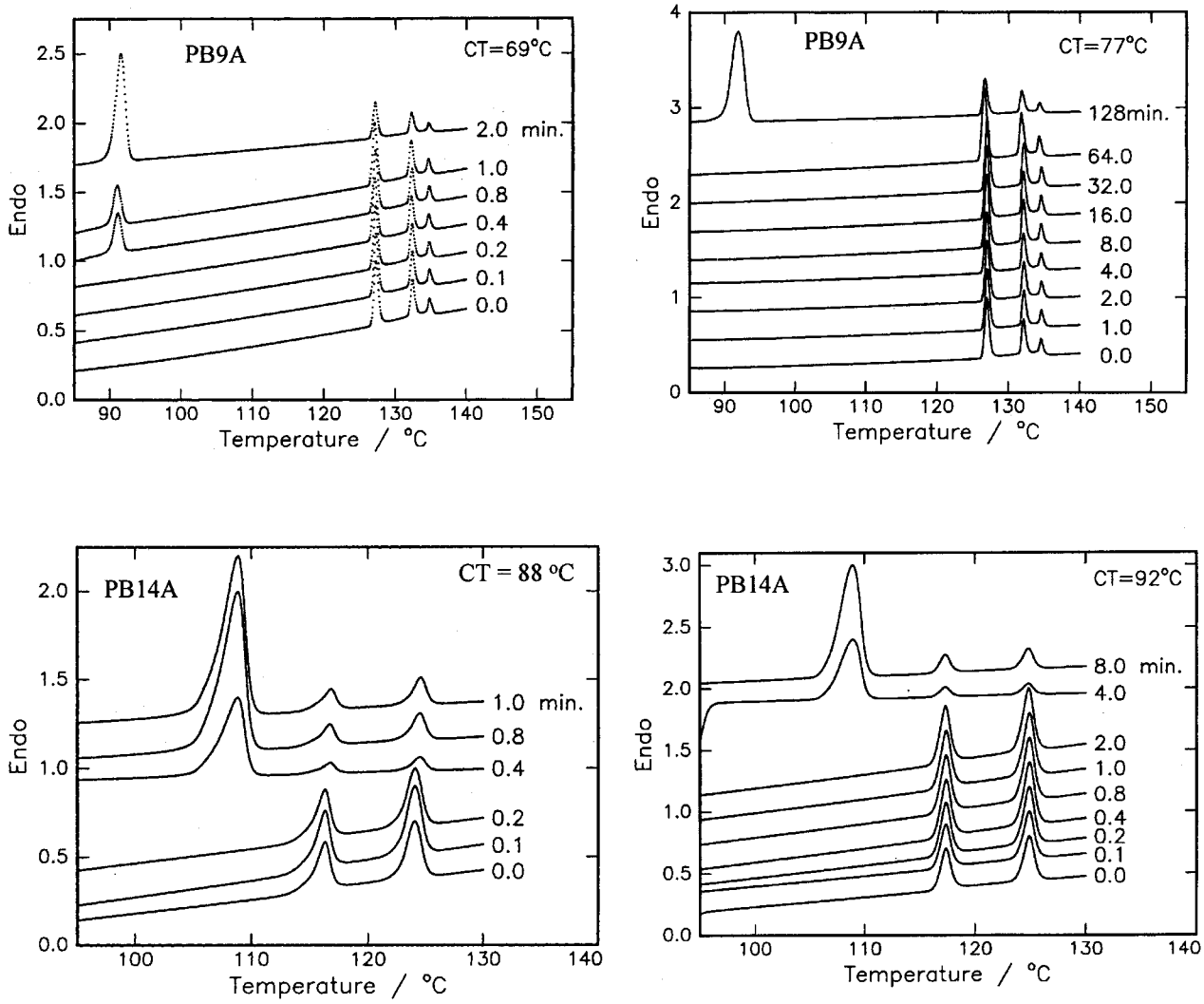

Figure 3. DSC endotherm profiles of PB*n*A compounds.

further implied from the delayed crystallization mechanism, which is equally manifested by both temperature and time.

3.1.1.2. *p-Phenylbenzylidene-p′-tetradecylaniline (PB14A).* Relating to the transitions from the kinetophase (SmB), the crystallization kinetics was selectively performed at the crystallization temperatures 88, 89, 90, 91 and 92°C. Typical endotherm profiles recorded at crystallization temperatures, 88 and 92°C are presented in figure 3.

The heating curve recorded after holding the compound at 88°C for a time interval of $t = 0$ min exhibits two distinct transitions with the absence of a crystal to melting transition. However, at $t = 0.4$ min the sudden appearance of a melting transition suggests a very fast crystallization process. The saturated value of enthalpy is observed at $t = 1.0$ min. The endotherm profiles recorded at crystallization temperatures, 89, 90, 91 and 92°C for different time intervals show a similar trend of crystallization kinetics, and the saturated values of enthalpy are obtained after 1.0, 2.0, 4.0 and 8.0 min, respectively. This trend suggests a slow rate of crystallization at the higher temperatures.

3.1.2. *p-Alkoxybenzylidene-p′-alkylanilines (nO.m)*

The *n*O.*m* class of liquid crystalline materials exhibit fascinating mesmorphic behaviour associated with convenient thermal ranges, which make them suitable candidates for systematic kinetic investigations. The prime objective of selecting the higher homologues of this series for crystallization kinetics was to study the effect of alkoxy terminal chains of the benzaldehyde moiety on the rate of crystallization. In addition, comparative analysis with the PB*n*A series may elucidate the influence of a bulky phenyl ring on the growth of crystallization.

To meet this requirement, two representative *n*O.*m* compounds were selected so that the carbon numbers of the alkylaniline moieties are equal to 9 and 14 as, i.e. 18O.9 and 15O.14.

3.1.2.1. *p-Octadecyloxybenzylidene-p′-nonylaniline (18O.9).* From the temperature difference between the melting and crystal transitions, the crystallization kinetics relating to transitions from the smectic F phase was performed over the crystallization temperatures, 48, 50, 52, 54 and 56°C at different time intervals. Figure 4 shows typical endotherm profiles recorded at crystallization temperatures 48 and 56°C.

The heating curve recorded at crystallization temperature 48°C with a time delay of $t = 0$ min displays the SmF–I transition only. The sudden appearance of a crystal to melting transition is observed after holding the sample for 2.0 min, exhibiting a fast rate of crystallization. The formation of this melting transition increases with increase in time interval, and its growth continues until the time interval reaches 4.0 min. This process of crystallization can be accounted for on the basis of larger and larger crystal fractions with time, complete after 8.0 min. The endotherm profiles recorded at crystallization temperatures 50, 52, 54 and 56°C for different time intervals show a similar trend of crystallization kinetics and saturated values of enthalpy are obtained after 8.0, 16.0, 32.0 and 120.0 min, respectively. This trend, however, implies a homogeneous process of crystallization with a unique mechanism operating through the entire thermal span.

3.1.2.2. *p-Pentadecyloxybenzylidene-p′-tetradecylaniline (15O.14).* As borne out by the heating and cooling thermograms (figure 2), the crystallization kinetics was selectively performed at the crystallization temperatures 62, 64, 66 and 68°C. Typical endotherm profiles recorded at 62 and 68°C are represented in figure 4.

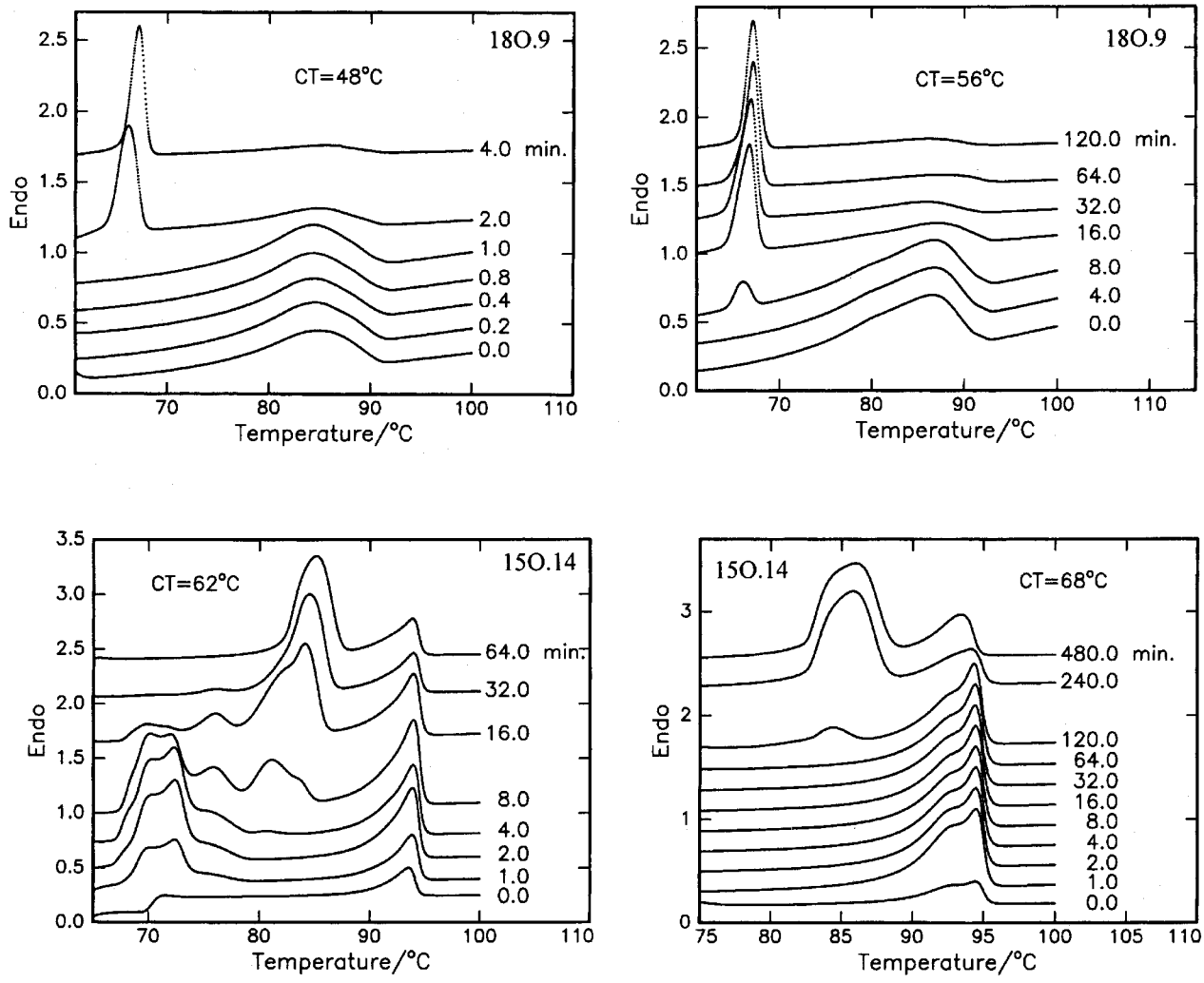

Figure 4. DSC endotherm profiles of *n*O.*m* compounds.

The endotherm recorded at the initial crystallization temperature 62°C, with a time delay of $t = 0$ min, displays the G–I transition following the quenching of the crystal to melting transition. The growth of the melting transition follows a different trend from 18O.9. After holding the sample for 1.0 min, the formation of a melting transition starts as a small peak at 72°C. This peak is designated as a *pseudo melting transition*, and may be attributed to the formation of two molecular fragments originating from a molecular strain on the central rigid core (>C=N) due to the long carbon chain on either side. The growth of this peak increases with time and reaches its maximum enthalpy value of 47.0 J g^{-1} at a time interval of 8.0 min. It should be noted that the endotherm profile at this time interval shows the formation of a melting transition at 81.6°C. This endotherm profile is critical in the sense that both the fragments are in an equilibrium state. The formation of this melting transition increases with time, and a simultaneous quenching of the peak corresponding to the pseudo melting transition is observed until the time interval reaches 64.0 min. At this juncture, it is useful to recall the similar trend in the growth of melting transitions in our previous reports [6] on the analogous members of the *n*O.*m* series, 11O.16 and 16O.16, where the growth of the melting transition proceeds at the expense of a pseudo melting transition leading to a complicated process of crystallization. Hence, it is quite reasonable to predict that a delayed process of crystallization is favoured when a linear molecule possess long terminal carbon chains on either side of the central rigid core (>C=N−).

The endotherm profiles recorded at crystallization temperatures 64 and 66°C for different time intervals show a similar trend in the formation of a melting transition, and the saturated enthalpy values are obtained after 64.0 and 120.0 min, respectively. On the other hand, the endotherm profiles obtained at 68°C (figure 4) show the non-existence of a pseudo melting transition at lower temperatures, suggesting the stabilization of one molecular fragment upon re-orientation of molecular arrangements. The saturated enthalpy value is obtained after holding the sample for 480.0 min.

3.2. *Process of crystallization*

In general, the kinetics of crystallization involving the rate of growth of small domains in a smectic phase is equally manifested by its characteristic temperature and time. The particular case of a temperature dependent nucleation mechanism, which takes place as a homogeneous process over a constant period of time, leads to the sporadic growth phenomenon. However, during this process, the contributions from crystal defects, impurities and solid state transformations play an effective role on the overall rate of phase transformation and the dimensional geometry of the growing domains [4].

In order to study the trend of crystallization mechanism at each crystallization time, the enthalpy values for individual transitions at different time intervals were calculated at each crystallization temperature and the corresponding data plotted against the corresponding logarithm of time interval for each compound in present study.

3.2.1. *p-Phenylbenzylidene-p′-alkylanilines (PBnA)*

The heats of transitions for individual transitions for different time intervals were calculated at each crystallization temperature and the data plotted against log of time interval for each compound (table 2). Figure 5 shows these plots for PB9A and PB14A. At 69 and 77°C, PB9A plots are of identical shape, apart from the shift in the log t axis, suggesting the limitations of rate of crystallization [4, 6]. Moreover, the simultaneous measurement of ΔH of the SmB endotherm with time, illustrates the effective beginning and end to the crystal formation process which coincides with the formation of the melting transition. The plot of ΔH of the growing melting transitions against log annealing time at different crystallization temperatures (69–77°C), obtained by shifting the data along log t axis, is also depicted in figure 5. A glance at this master curve clearly shows a sudden increasing trend in ΔH values for higher crystallization temperatures, providing substantial evidence for the existence of two different crystallization mechanisms operating over the entire crystallization thermal range. However, figure 5 also shows a sudden increasing trend in the ΔH values for PB14A at higher crystallization temperatures. This indicates the existence of a unique nucleation mechanism, which controls the overall crystallization process in these compounds.

3.2.2. *p-Alkoxybenzylidene-p′-alkylanilines (nO.m)*

Similar plots have been constructed for 15O.14 and 18O.9 using ΔH values for individual transitions for different time intervals, calculated at each crystallization temperature, see figure 6. The plots are identical, which reveals the existence of a uniform crystallization mechanism over the entire thermal range. Apart from the shift in the log t axis, the identical shapes suggest the limitations of rate of crystallization [4, 6]. On the other hand, the ΔH vs. log t curves plotted for 18O.9 clearly show a sudden increasing trend in ΔH value for higher crystallization temperatures; this indicates that two different crystallization mechanisms operate over the entire crystallization thermal range as in the case of PB*n*A compounds. Nevertheless, the overall crystallization rate at the saturation is controlled by a nucleation rate and the rate of growth of domains [7–10].

Table 2. Measured crystallization parameters from different kinetophases in PB*n*A and *n*O.*m* compounds.

Compound	Kinetophase	Crystallization temperature/°C	Crystallization time (t^*)/min	x	n	b
PB9A	B	69	2.0	0.9912	2.36	0.193
		71	4.0	0.9989	1.12	0.209
		73	8.0	0.9989	0.85	0.168
		75	8.0	0.9924	0.61	0.280
		77	128.0	0.9998	0.07	0.711
PB14A	B	88	1.0	0.9908	4.69	10.0
		89	1.0	0.9946	5.22	10.0
		90	2.0	0.9512	1.51	0.351
		91	4.0	0.9491	0.74	0.356
		92	8.0	0.9457	0.36	0.468
18O.9	F	48	4.0	0.9730	0.90	0.285
		50	8.0	0.9802	0.49	0.360
		52	16.0	0.9919	0.30	0.434
		54	32.0	0.9836	0.13	0.639
		56	120.0	0.9795	0.03	0.856
15O.14	G	62	64.0	0.9908	0.07	0.736
		64	64.0	0.9905	0.07	0.738
		66	120.0	0.9703	0.03	0.869
		68	480.0	0.9664	0.007	0.957

3.3. *Nucleation mechanism*

It is well known that the process of crystallization involving the fraction of transformed volume x at the time interval t from the beginning of the crystallization process is expressed in terms of the Avrami equation [14, 15]

$$x = 1 - \exp(-bt^n) \tag{1}$$

where the constants b and n depend on the nucleation mechanism and the dimensional geometry of the growing domains, respectively. The data for all the crystallization temperatures can also be obtained from the single equation [4],

$$x = 1 - \exp[-(t/t^*)^n] \tag{2}$$

where $t^* = b^{-1/n}$. Further, the characteristic time t^* can be determined experimentally at $t = t^*$; x at a particular crystallization temperature is deduced from the experimental data of $\Delta H/\Delta H_o$, where ΔH is the crystal melting heat measured at characteristic time t and ΔH_o is the maximum value obtained from the plateau of individual master curves (figures 5 and 6). Substituting these values of t^* and x in equation (1), constants b and n are obtained at a specified crystallization temperature. The values of n calculated from equation (2) for all the compounds are included in table 2.

3.3.1. *Dimensionality parameter, n*

It is well established that the magnitude of the Avrami exponent n plays a crucial role in ascertaining the mode and class of rate transformations, which occur when a stable low temperature phase grows out of a mother metastable phase in the form of small domains [16]. In the PB*n*A series, the value of n varies from 0.07 to 2.3 (PB9A) and from 0.3 to 5.2 (PB14A). It is evident from the degree of variation of n (at a particular crystallization temperature), that the compound exhibits an independent nucleation mechanism. A possible explanation for this anomalous crystallization behaviour is the ocurrence of sporadic nucleation growth, which follows an inhomogeneous process of continuous nucleation over a constant time [4, 6]. These values (table 2) clearly suggests that a different trend in the conversion process is followed at each crystallization temperature. Hence, it is reasonable to assume that the compounds follow two stages in the conversion process: *diffusion controlled transformation* (for n ranging from 0.5 to 2.5), where particles are nucleated only at the start of transformation and which proceeds at a constant rate; and *cellular (diffusionless) transformation* (for $n > 4$) in which nucleation occurs with an increasing rate at grain boundaries [16]. The varied magnitude of n may also be influenced by either a two-dimensional sporadic nucleation or by growth in three dimensions. The former is more conductive for the crystallization process to occur in smectic layers [7–10].

In the case of *n*O.*m* compounds (table 2), the value of the exponent n varies from 0.007 to 0.073 in 15O.14, and from 0.032 to almost unity in 18O.9. The value of the dimensionality parameter n varies at each crystallization temperature and follows a decreasing trend with increasing temperature. Further it is evident from the degree of variation in this parameter (at a particular

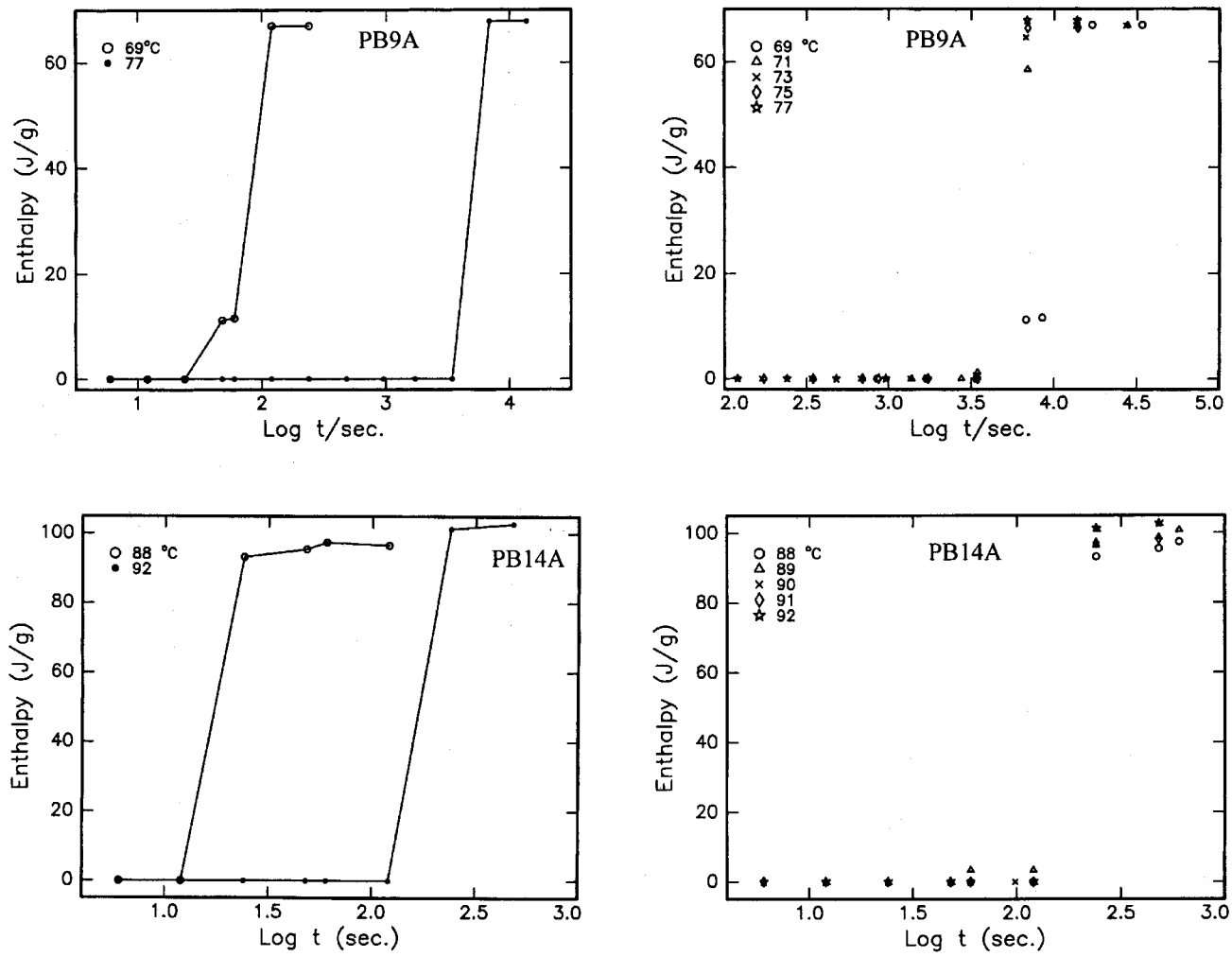

Figure 5. Heats of melting vs. log of annealing time in PB*n*A compounds.

crystallization temperature) that these compounds also exhibit an independent conversion process. It is also worth mentioning that the alkyl terminal chain plays a dominant role on the crystallization time at a particular crystallization temperature. These values (table 2) suggest that the mode of conversion falls in the category of diffusion-controlled transformations, leading to a situation similar to first order kinetics, which involves the growth of isolated plates or needles of finite size [16]. Moreover, the possible explanation for the magnitude of n may include either a two-dimensional sporadic nucleation or growth in three dimensions.

3.3.2. *Nucleation growth parameter, b*

The values of constant b, which governs the nucleation mechanism, are calculated for these compounds and included in table 2. Its magnitude in the PB*n*A series is unaltered with an order of 10^{-1} at most of the crystallization temperatures. The trend in the magnitude of b is in good agreement with reported data of analogous smectogens [7–10].

In the individual cases of *n*O.*m* compounds, 15O.14 and 18O.9, the constant b shows an altogether different trend of magnitudes. It is interesting to note that the values (with an order of 10^{-1}) obtained for each of the compounds show a gradual increment with increasing crystallization temperature (table 2). The occurrence of this trend may be accounted for on the basis of the existence of a unique crystallization mechanism operating over the entire crystallization thermal ranges.

A quantitative approach has been made to study the effect of alkyl chain length on crystallization behaviour, in terms of the varied magnitudes of constant b, by constructing the plot of $\log b$ at different crystallization temperatures for all the compounds. The corresponding

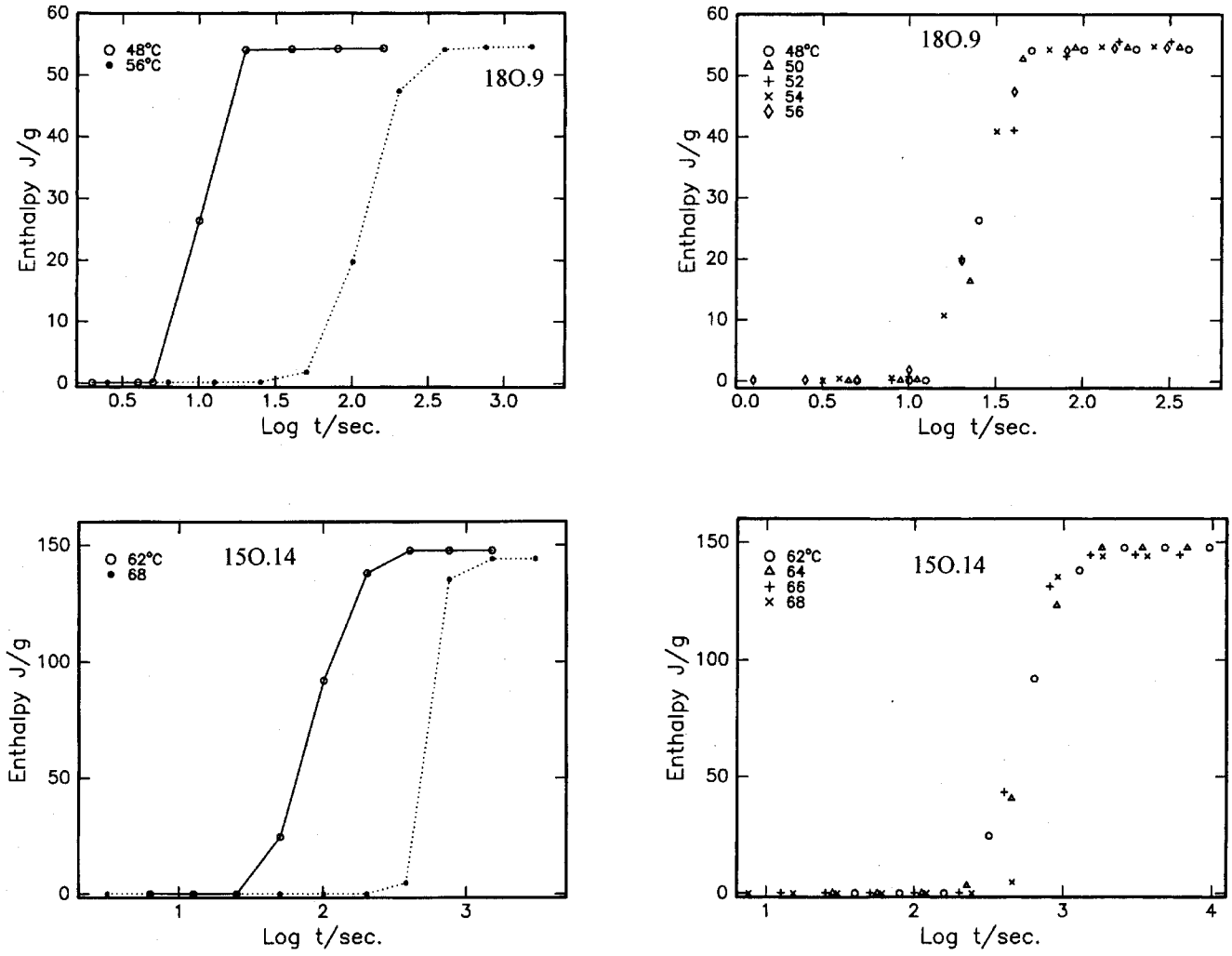

Figure 6. Heats of melting vs. log of annealing time in *n*O.*m* compounds.

slope values for each member is obtained by a linear fit, which is performed to the respective values of log b and crystallization temperatures (figure 7). However, in the case of PB14A the b values at 88 and 89°C are ignored while fitting the data, as the substitution of exponential powers of time intervals of 1.0 min in the equation, $b = 1/t^n$ leads to a constant value of 1.00. Figure 7 shows an increasing trend in the slope magnitude. It is now clear that the alkoxy chain length has a pronounced effect on the nucleation mechanism. In other words, the presence of terminal phenyl rings promotes a fast rate of crystallization. Moreover, the range of crystallization temperatures of the series broadens with the increase of alkoxy chain length. Nevertheless, the linear nature of the curves strongly implies a unique crystallization process that operates over the entire thermal range of the individual compound.

3.3.3. *Influence of kinetophase on crystal growth mechanism*

The phase sequence in the smectogens has a pronounced influence on the crystallization kinetics. In fact, the 'kinetophase', which occurs prior to crystallization, plays a crucial role in determining the rate of crystallization. Our extensive experimental studies [6] on different *n*O.*m* compounds exhibiting various kinetophases enables us to arrange them in the increasing order of crystallization time in orthogonal and tilted kinetophases:

$$\mathrm{SmB} < \mathrm{SmA}$$

$$\mathrm{G} < \mathrm{SmF} < \mathrm{SmI} < \mathrm{SmC}$$

This order implies that the kinetic rate is fast for kinetophases towards the crystal end of the phase range, and slow for those near the isotropic melt.

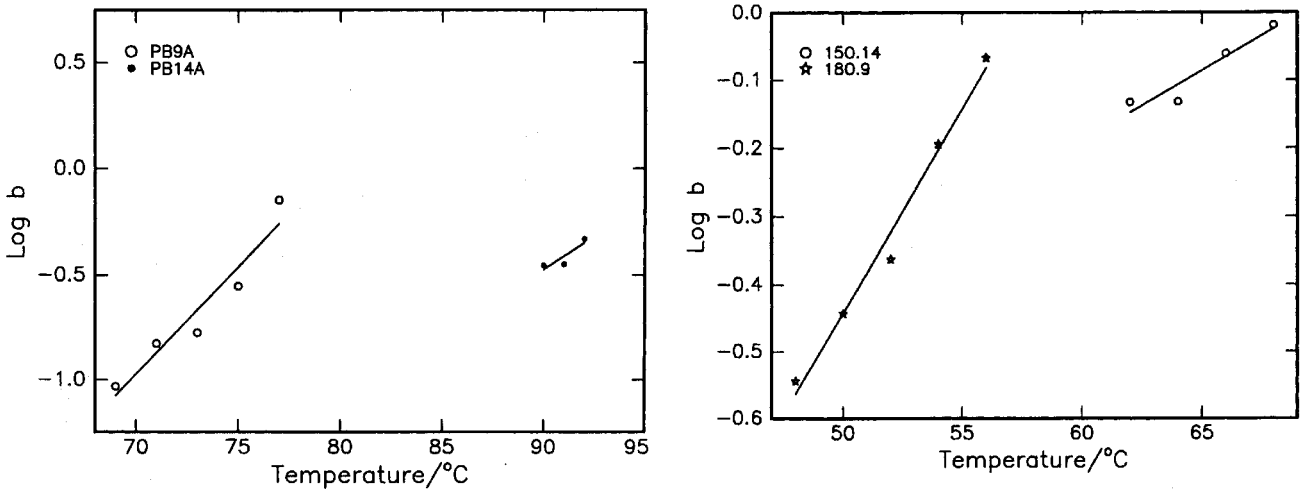

Figure 7. Log b as a function of crystallization temperature for PBnA and nO.m compounds.

In this section we have made a qualitative approach to the nucleation process in smectogens of both tilted and orthogonal categories. It is well known that molecules in the orthogonal smectic phases are parallel to each other with their long axes perpendicular to the layer plane, resulting in free rotation of the molecule around the long molecular axis [17]. Consequently, in the case of a tilted phase the significant difference is the tilt of the molecular long axes with respect to the layer normal, leading to hindered rotation of the molecule along the long axis [17]. Moreover, the layer thickness in a tilted mesophase is smaller than the molecular length ($d < 1$) while in the case of orthogonal ordering they are approximately equal. This degree of variation in the layer thickness, together with molecular rotation, has a striking influence on the rate of crystallization process.

It is seen from the present experimental studies (table 1), that the values of heat of transitions (ΔH) for a given tilted (G/SmF) and orthogonal (SmB) to crystal transition show two distinct values, and that these ΔH values are relatively smaller in orthogonal kinetophases than in tilted phases. It is now clear that the process of crystallization in an ordered kinetophase requires a relatively high thermal energy, because it is partially distributed between the molecules and the corresponding layers. Moreover, the growth of ordered nuclear domains in an orthogonal kinetophase may follow at faster rates due to the free molecular motions within the smectic layers. The lower ΔH values for transformations in orthogonal phases speaks volumes about the fast crystallization process. Based on these underlying facts observed from the experimental data on various smectogens [6–10], we are able to correlate the relative magnitude of ΔH with the rate of crystallization. From this relationship, we propose that these kinetophase transformations that involve low magnitudes of ΔH promote a faster rate of crystallization, while those with high ΔH support delayed crystallization times.

3.3.4. *Formation of a stable nucleus*

The formation of an ordered domain occurs first, and then converts to a stable nucleus that initiates the aggregation of surrounding molecules to form layered domains. The origin of the nucleus is critical because formation of a seed nucleus proceeds until it reaches a sufficient size to initiate the crystallization process. It is proposed that this process of crystallization is controlled by the lamellar and interlayer distances in non-tilted and tilted kinetophases, respectively. In such a process of seed nucleation, the factors related to the smectic layers play a crucial role. In a particular smectic layer the molecule first acquires the requisite internal energy to allow formation of ordered domains, which propagates crystallization in the adjacent smectic layers. These ordered domains further proceed in a smectic layer by a process of successive addition of the molecules from neighbouring layers, leading to sporadic nucleation and growth in two dimensions. This crystallization process then continues until the crystallization is completed.

The mode of crystal conversion in a tilted smectic layer is rather a complicated and delayed process due to the hindered motion of the molecules. In an orthogonal kinetophase the initialization of the crystallization process primarily begins with the annihilation of short-range forces, with the subsequent formation of new long-range forces; this triggers the completion of the crystallization in a fast crystallization time. These underlying facts are experimentally realized in the present study by the delayed crystallization process in tilted kinetophases (G and SmF) when compared with that in the orthogonal kinetophase (SmB).

4. Conclusions

The experimental results on comparative crystallization kinetics performed on different smectogens of the classes PB*n*A and *n*O.*m* are summarized as follows:

(1) The crystallization kinetics experiments performed on each series of the present compounds reveals different trends of crystallization behaviour among individual members of each series.
(2) At final crystallization temperatures, the smectogens are found to exhibit a slow rate of kinetics.
(3) The influence of a phenyl ring as a terminal moiety is seen in a fast rate of crystallization.
(4) An increase in alkoxy carbon numbers at the aniline moiety delays crystallization time.
(5) Thermal spans of crystallization temperatures are found to be greater for the higher homologues of the series.
(6) The magnitudes of the Avrami parameters n and b suggest that a unique crystallization mechanism operates over a particular crystallization time.
(7) Low values of n infer the occurrence of diffusion-controlled transformations in which nucleation starts as an initial growth of particles in the form of plates or needles of finite size possessing impinged edges.
(8) The degree of variation in the dimensionality parameter n at each crystallization temperature demonstrates an independent nucleation mechanism for any individual member of the series.
(9) In most of the cases, the magnitude of constant b, which governs the nucleation mechanism, is unaltered with an order of 10^{-1}. The linear nature of $\log b$ vs. CT curves strongly implies a unique method of the crystallization process.
(10) Comparative studies reveal a profound influence of the nature of the kinetophase on the rate of crystallization.

This work was supported by the Council of Scientific and Industrial Research, 13(7544-A)/2000-Pool, and Department of Science and Technology (SP-S2M-45/94) New Delhi.

References

[1] Budgell, D. R., and Day, M., 1991, *Polym. Eng. Sci.*, **31,** 1271.
[2] Minkova, L. I., and Magagnini, P. L., 1995, *Polymer*, **36,** 2059.
[3] Tieh, M. H., and Feng-Chih, C., 2000, *J. polym. Sci. B*, **3,** 934.
[4] He, Z., Zhao, Y., and Caille, A., 1997, *Liq. Cryst.*, **23,** 317.
[5] Liu, S. L., Chung, T. S., Torii, Y., Oikawa, H., and Yamaguchi, A., 1998, *J. polym. Sci. B*, **36,** 1679.
[6] Kumar, P. A., Madhu Mohan, M. L. N., and Pisipati, V. G. K. M., 2000, *Liq. Cryst.*, **27,** 727.
[7] Swathi, P., Kumar, P. A., and Pisipati, V. G. K. M., 2001, *Liq. Cryst.*, **28,** 1163.
[8] Srinivasulu,M., Satyanarayana, P. V. V., Kumar, P. A., and Pisipati, V. G. K. M., 2001, *Liq. Cryst.*, **28,** 1321.
[9] Srinivasulu,M., Satyanarayana, P. V. V., Kumar, P. A., and Pisipati, V. G. K. M., 2001, *Mol. Mater.*, **14,** 215.
[10] Swathi, P., Kumar, P. A., and Pisipati, V. G. K. M., 2001, *Z. Naturforsch.*, **56a,** 692.
[11] Rao, N. V. S., and Pisipati, V. G. K. M., 1984, *J. phys. Chem.*, **87,** 884.
[12] Potukuch, D. M., Lakshminarayana, L., Prabhu, C. R., and Pisipati, V. G. K. M., 1996, *Cryst. Res. Technol.*, **31,** 685.
[13] Gray, G. W., and Goodby, J. W. G., 1984, *Smectic Liquid Crystals: Textures and Structures* (London: Leonard Hill).
[14] Avrami, M., 1939, *J. chem. Phys.*, **7,** 1103.
[15] Avrami, M., 1940, *J. chem. Phys.*, **8,** 212.
[16] Rao, C. N. R., and Rao, K. J., 1978, *Phase Transitions in Solids* (McGraw-Hill).
[17] Demus, D., 1994, *Liquid Crystals: Phase Types, Structures, and Chemistry of Liquid Crystals* (New York: Springer).